Int. J. Electrochem. Sci., 13 **(2018)** 6537 – 6549, doi: 10.20964/2018.07.24

International Journal of
ELECTROCHEMICAL
SCIENCE
www.electrochemsci.org

Short Communication

Corrosion Behavior of 9 % Ni Steel for LNG Storage Tanks in 3.5 wt. % NaCl Solution

Ming Qin[1,2], *Weichen Xu*[1,3], *Lihui Yang*[1,3], *Yantao Li*[1,3,*]

[1] CAS Key Laboratory of Marine Environmental Corrosion and Bio-fouling, Institute of Oceanology, Chinese Academy of Sciences, Qingdao 266071, China.
[2] University of Chinese Academy of Sciences, Beijing 100049, China.
[3] Open studio for marine Corrosion and Protection, Qingdao National Laboratory for Marine Science and Technology, Qingdao 266071, China.
[*]E-mail: ytli@qdio.ac.cn

Received: 26 February 2018 / *Accepted:* 4 April 2018 / *Published:* 5 June 2018

The corrosion behavior of 9 % Ni steel in a 3.5 wt. % NaCl solution was investigated by electrochemical techniques including open circuit potential (OCP), potentiodynamic polarization, and electrochemical impedance spectroscopy (EIS). The principal components and morphology of 9 % Ni steel and the resulting corrosion layer are analysed by metallographic evaluation, scanning electron microscopy (SEM), energy-dispersive spectroscopy (EDS), Raman spectroscopy, X-ray diffraction (XRD) and Fourier transform infrared spectroscopy (FTIR). The results suggest that the anodic reaction is primarily the dissolution of the iron matrix and the cathodic process is mainly the reduction of oxygen. The corrosion resistance R_{ct} of 9 % Ni steel decreased with increasing immersion time and the corrosion layer did not provide protection. The outer section of the corrosion product consists mostly of lepidocrocite γ-FeOOH, trace goethite α-FeOOH, and magnetite Fe_3O_4. The inner section is a nickel-rich layer, which is related to the alloying elements and reverted austenite. Moreover, the corrosion layer was found to accelerate the selective corrosion.

Keywords: 9 % Ni steel; corrosion; electrochemical tests; reverted austenite; nickel-rich layer

1. INTRODUCTION

Because 9 % Ni steel has a special combination of high toughness and high strength even at extremely low temperatures (-196 °C), it has been used extensively as a material for the storage and transportation of natural gas[1-5]. Natural gas accounts for a significant proportion of energy production in today's world, and liquefied gas (LNG) is currently the fastest growing hydrocarbon fuel

in the world. It is also a clean source of energy with coal and oil, and they are known as the 'three pillars' of the world's energy. The importance of natural gas the global clean energy drives the development of natural gas industrial facilities[6]. Hydrostatic testing of the inner tank is required after construction for approximately 30 days. With the gradual increase in capacity of LNG storage tanks, the demand for tanker hydrostatic testing with freshwater has also increased. Due to the concept of 'green development', the LNG tank hydraulic test medium is gradually being replaced by seawater.

Because of the aggressive nature of seawater, the corrosion resistance of materials that are exposed to it is a major concern[7]. Carbon steel immersed in natural water often produces a layer of corrosion products on its surface[8]. Oxyhydroxides such as α-FeOOH, γ-FeOOH and β-FeOOH form in the rust layer depending on the environment [9-11]. Some iron oxides that form on the steel surface serve as a protective layer that slows down further corrosion, but some iron oxides do not prevent continuous steel loss[12].

Therefore, the use of seawater for hydrostatic testing presents the problem of seawater corrosion. Most research on 9 % Ni steel relate to its mechanical properties and heat treatments[13, 14], and very few papers report its corrosion characteristics in aqueous solution. With the continuous expansion of the global LNG industry, more storage tanks will also be developed. More and more large-capacity storage tanks will continue to be built on the coast. As the concept of global green development continues to gain strength, the use of seawater for hydrostatic testing of storage tanks will be emphasized. Global LNG green energy is developing at a rapid rate. Currently, there are few studies on the seawater corrosion of 9 % Ni steel. Therefore, research on the corrosion mechanisms of 9 % Ni steel in seawater is urgently needed. The purpose of this experiment is to study the corrosion characteristics of 9 % Ni steel in 3.5 wt. % NaCl solution to provide a reference for future engineering applications.

2. EXPERIMENTAL

2.1 Material and environment

The chemical composition of the 9 % Ni steel used is shown in Table 1. The 9 % Ni steel was treated by quenching and tempering. A sample was cut into 30 mm×20 mm×3 mm for the weightlessness test.

Table 1. Chemical compositions (mass %) of 9 % Ni steels

	Ni	C	Mn	Si	P	S	Fe
A553I	8.50~9.50	≤0.13	≤0.90	0.15~0.30	≤0.035	≤0.04	balance

For electrochemical measurements, a sample was cut into 10 mm×10 mm×5 mm and welded with copper wire, and then encapsulated in epoxy resin leaving a 10mm×10mm surface. Before electrochemical tests, the samples were successively ground by using 80, 240, 600, 800, 1000, 1500 grit sandpaper and washed with deionized water and ethanol. Finally, the samples were dried using flowing cold air and a dryer. For morphological examination, samples were mirror polished using a smooth cloth and 2.5μm alumina pasted. The solution (consist of sodium chloride and deionized water) contained 3.5 wt. % NaCl at 22±1 °C. For all the measurements, three or more parallel experiments were conducted.

2.2 Mass loss tests

The corrosion rate was measured by the mass loss method. The treated sample was placed in a 3.5 wt. % NaCl solution. After 30 days, the sample was taken out, derusted, washed with deionized water and alcohol, dried, and weighed. The rust removal solution contained identical volumes of deionized water, industrial hydrochloric acid and 3.5 g/L hexamethylenetetramine[15]. Using the measured sample weight change, the corrosion rate was calculated by the following formula:

$$\Delta\upsilon = \frac{\Delta m}{St}$$

where Δυ (g/m^2h) is the corrosion rate, Δm (g) is the difference between the mass of the sample before corrosion and its mass after removal of the corrosion products, S (m^2) is the surface area of the sample, and t (h) is the test time.

2.3 Electrochemical tests

Electrochemical tests were carried out using a Princeton PARSTAT 2273 electrochemical system. The work electrode, counter electrode and reference electrode consisted of the 9% Ni steel sample, a platinum foil and a saturated calomel electrode (SCE), respectively. The electrochemical corrosion behavior of the specimen was examined by open circuit potential (OCP), electrochemical impedance spectroscopy (EIS) and potentiodynamic polarization[16] in 3.5 wt. % NaCl solution.

The first step was to conduct an OCP test for 3h, waiting until the system was relatively stable (when the OCP value changed less than 5 mV in 600 s). When the test system reached a on steady-state OCP, the EIS measurement was conducted. The signal presented an amplitude of 10 mV and a frequency ranging from 100 kHz to 10 mHz. Potentiodynamic polarization curves were obtained ranging from -350 mV to +350 mV at a scan rate of 0.33 mV/s[17].

2.4 Morphology and composition analysis

The metallographic structure of the sample was analysed using an XYU-65C optical microscope. The surface of the metallographic specimen was brushed, polished, and etched in a 4 % aqueous solution of Nital to reveal the microstructure. The microscopic morphology of the sample was

observed using scanning electron microscopy (SEM, JEOL-JSM-5600) combined with energy dispersive X-ray spectroscopy (EDS, Oxford Instruments INCA) after immersion in solution for 30 days.

Corrosion products were collected, dried and ground to powder after the weightlessness test. The composition of the corrosion products was acquired by X-ray diffraction, Raman spectroscopy and Fourier transform infrared spectroscopy. XRD patterns were obtained on an Ultima IV diffractometer (Rigaku) operated at 40 kV and 40 mA with Cu-Kα (λ=1.5418 Å) radiation, a scan range of 10°-80° and a scan rate of 10°/min. Raman spectra of the corrosion products were recorded by a custom-designed N-RXNE-532-RA-SP spectrometer (Kaiser Optical Systems, Inc.). FTIR spectroscopy was performed using a Vertex 70 FTIR (Bruker).

3. RESULTS

3.1 Metallographic examination

The metallographic structure of the 9 % Ni steel consisted of martensite with some reverted austenite (Fig. 1). Ni and Mn are conductive to the stability of austenite and reverted austenite is rich in Ni. It is generally believed that the low temperature toughness of 9 % Ni steel can be attributed to the austenite formed during tempering[18, 19].

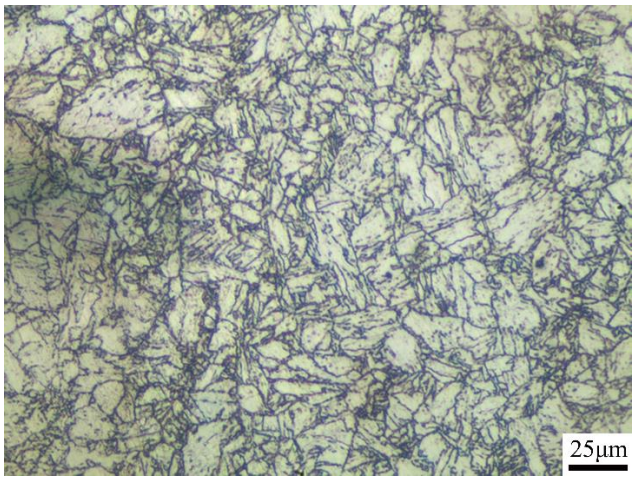

Figure 1. The microstructure of 9 % Ni steel

Previous studies have shown[20] a relationship between the microstructure and the corrosion resistance of steel. Austenite is a solid solution of carbon in γ-Fe and has a face-centred cubic structure, while martensite is a supersaturated solid solution of carbon inα-Fe and has a body-centred cubic structure. Martensite is generally obtained through a quenching process. Due to rapid cooling, the supersaturated carbon dissolves in the matrix and the microstructure is not stable. Carbon and various impurities are segregated at room temperature. Corrosion can then easily initiate at a large number of dislocations and micro-cracks in martensite.

3.2 Electrochemical tests

Electrochemical tests were conducted to investigate uniform and localized corrosion of 9 % Ni steel. The sample was immersed in 3.5 % NaCl. As reported[21, 22], a decreasing OCP is indicative of the generation and development of corrosion, whereas a relatively stable OCP indicates a balance between the dissolution and deposition of corrosion products. The OCP measured decreased with time (Fig. 2). This could have been active dissolution throughout the process. When the dissolution and deposition of corrosion products reached an equilibrium after 3h, the OCP value stabilized at around -0.53 V_{SCE}.

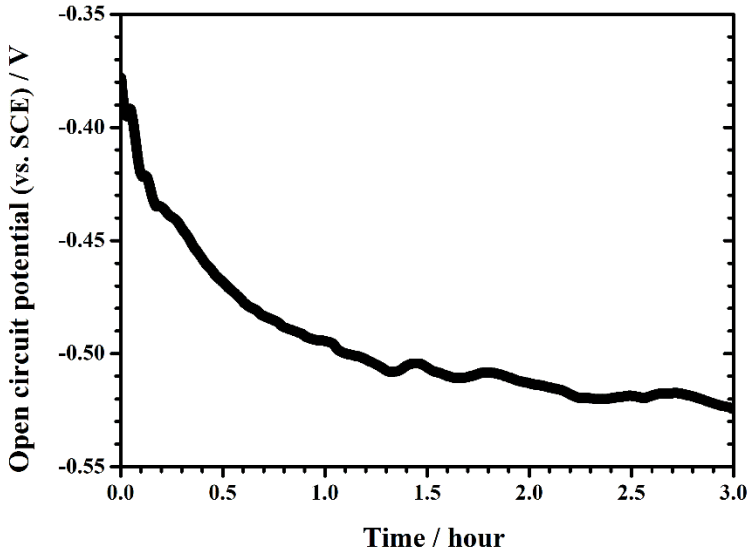

Figure 2. The open circuit potential of 9 % Ni steel in 3.5 wt. % NaCl

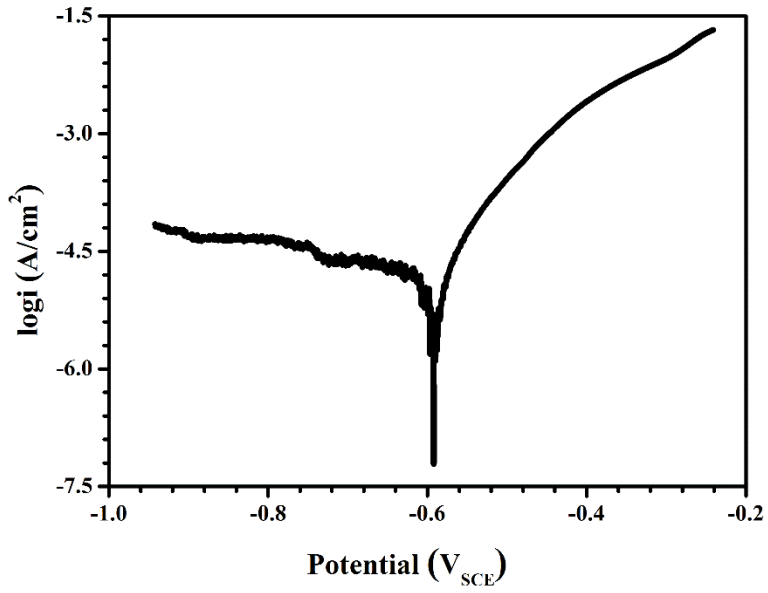

Figure 3. The potentiodynamic polarization curve of 9 % Ni steel in 3.5 wt. % NaCl

To further analyse the kinetics of 9 % Ni steel in 3.5 wt. % NaCl solution, a potentiodynamic polarization test was conducted. The polarization curve reveals the relationship between the electrode potential and the polarization current density[23]. The average corrosion rate from the potentiodynamic polarization measurement is shown in Fig. 3. The anodic reaction showed active dissolution mainly of the Fe-matrix. The cathodic process seemed to be an oxygen reduction reaction. In general, the self-corrosion potential indicates the corrosion tendency of a material the more negative the potential, the greater the corrosion tendency. Fitting the polarization curve shows that the self-corrosion potential was -0.59 V_{SCE} in 3.5 wt. % NaCl solution, and the polarization current density value was 1.72×10^{-5} A/cm^2. Linearly polarized resistance is calculated as 0.963×10^{-4} Ω·cm^2.

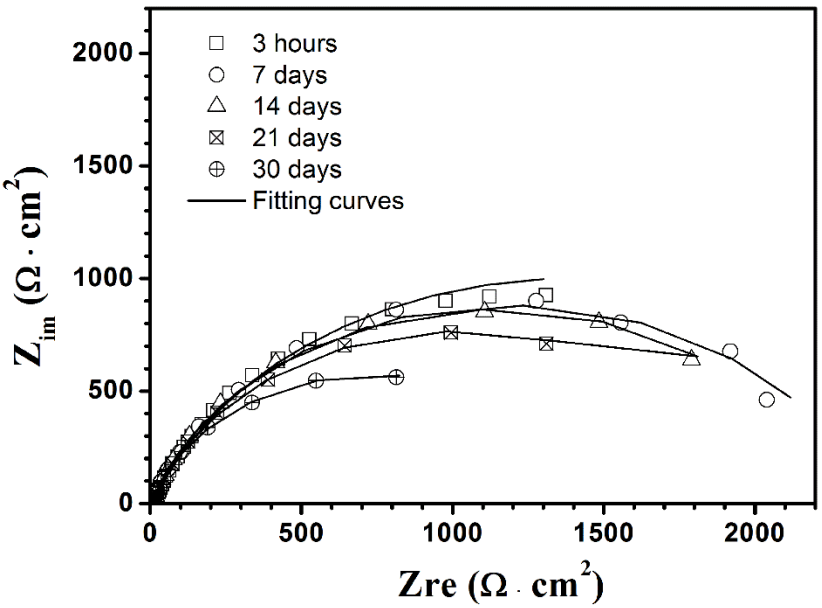

Figure 4. Nyquist diagrams of 9 % Ni steel during immersion in 3.5 wt. % NaCl for 3 h, 7 d, 14 d, 21 d, 30 d

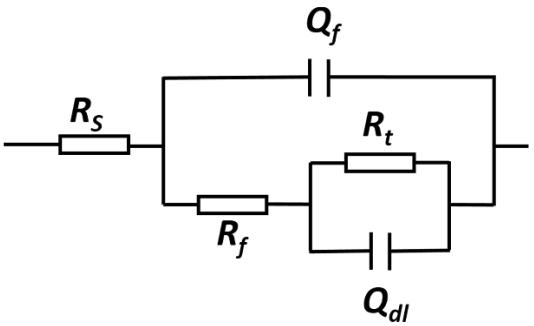

Figure 5. Equivalent circuits after immersion for 3 h, 7 d, 14 d, 21 d, 30 d

The cathodic reaction of 9% Ni steel in 3.5 wt. % NaCl could be described as three stages (Fig.3). In the first stage, the reaction is dominated by the oxygen reduction reaction in solution and is controlled by the electrochemical process. In the second stage, as the reaction progresses, oxygen is gradually consumed and oxygen elsewhere in the solution cannot reach the metal surface, so the

oxygen diffusion process dominates. In the third stage, the cathode polarization potential becomes more negative, and reaches the hydrogen evolution potential, and then the hydrogen evolution reaction occurs. The hydrogen embrittlement failure of metal is induced by the hydrogen evolution reaction. Moreover, in cathodic protection applications[24, 25], hydrogen evolution reactions also consume part of the applied current and result in energy waste.

Electrochemical impedance spectroscopy can be used to study the relevant steps of corrosion reactions and reveal the electrochemical mechanisms of corrosion in 3.5 wt.% NaCl solutions[21, 26, 27]. Nyquist curves obtained from 9 % Ni steel in 3.5 wt.% NaCl solution for 3 h, 7 d, 14 d and 30 d are shown in Fig.4. The Nyquist diagrams for each time period showed similar capacitive arc curves. The capacitive arc radius decreased as the immersion time in 3.5 wt. % NaCl solution increased, indicating that the corrosion rate accelerated with increasing immersion time. The corrosion process continued to extend after 30 days.

Table 2. Fitting parameters of equivalent circuits

Time	R_S /Ω·cm^2	Q_f-Y$_0$ /10^{-3}·S·cm^2	Q_f-n	R_f /Ω·cm^2	Q_{dl}-Y$_0$ /10^{-3}·S·cm^2	Q_{dl}-n	R_t /Ω·cm^2
3 hours	4.566	1.297	0.7663	9.192	2.241	0.8067	2792
7 days	1.168	3.261	0.9069	6.183	6.639	0.7659	2388
14 days	5.192	7.476	0.8353	6.512	1.082	0.8246	2262
21 days	5.013	1.111	0.8156	5.977	2.087	0.8203	2043
30 days	4.887	2.295	0.8374	3.967	3.737	0.8386	1479

The equivalent circuit shown in Fig.5 was used to calculate the fitting parameters from the Nyquist diagram[27]. Here, R_s is the solution resistance. In the electrolyte / corrosion products film interface, a double layer occurred, which is represented by a combination of a constant phase element (Q_{dl}) and the charge transfer resistance (R_t). The capacitor of the corrosion products film is represented by a constant phase element (Q_f), and R_f represents the resistance of the corrosion products film. Fitting parameters are shown in Table 2; the longer the immersion time, the smaller the R_t value. This indicated the absence of a dense protective layer on the metal surface. Due to the non-uniformity of metallographic of 9 % Ni steel, many micro batteries were formed and the corrosion was accelerated.

3.3 Mass loss and corrosion morphology analysis

The corrosion rates of the samples were measured by the mass loss method after immersion in 3.5 wt. % NaCl solutions for 30 days. The average corrosion rate and average corrosion depth were 0.627 g/m^2•h and 0.0696 mm/a, respectively.

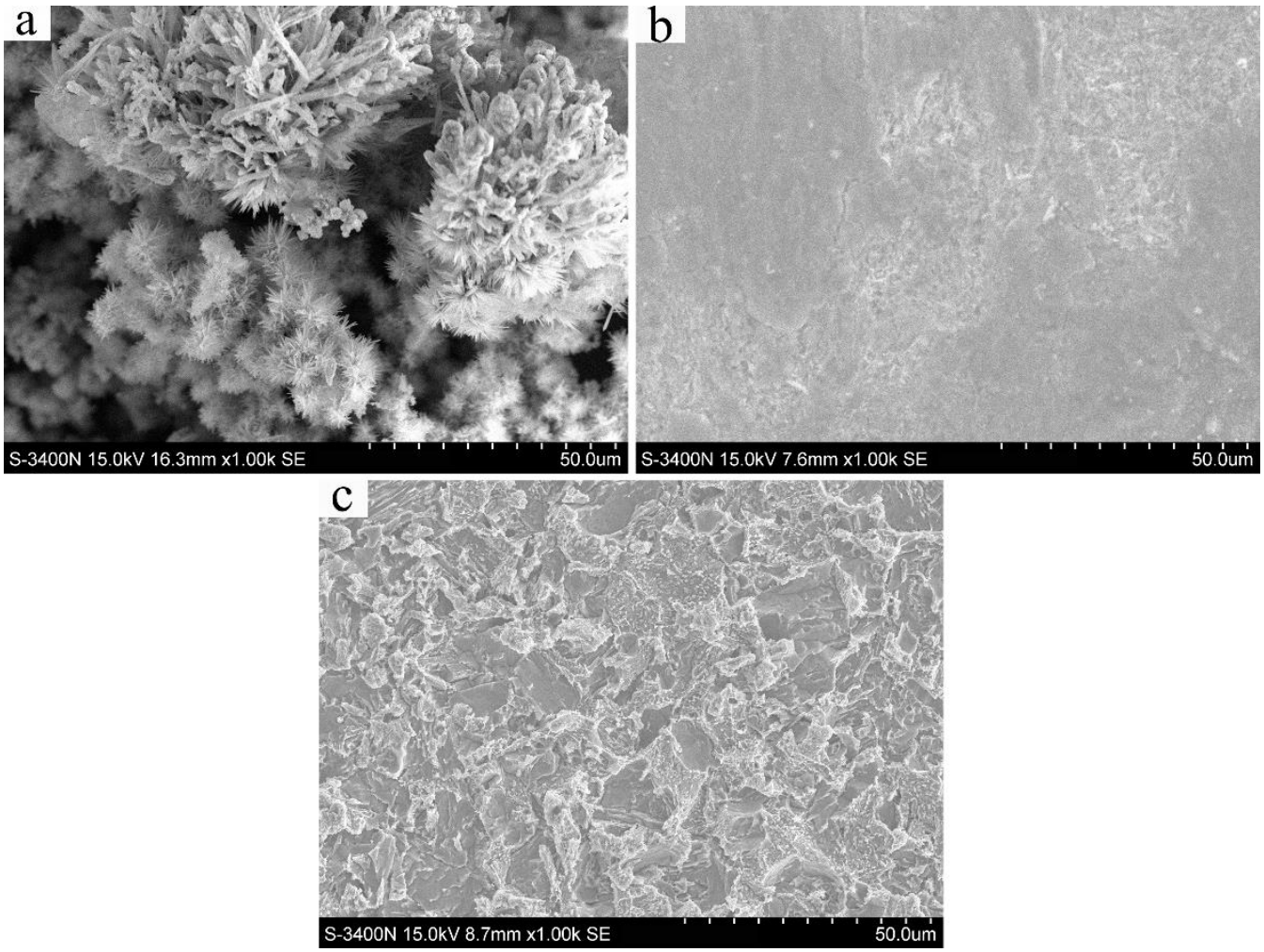

Figure 6. Corrosion morphologies of 9 % Ni steel after immersion in 3.5 wt. % NaCl for 30 days: (a) outer layer, (b) inner layer, (c) the surface after corrosion products were removed

Corrosion morphology analysis of 9 % Ni steel was performed after 30 days of immersion in 3.5 wt. % wt. NaCl solution (Fig. 6); the outer layer was covered by corrosion products (Fig. 6a). The appearance of the layer was fairly uniform with a red-brown colouring. Lepidocrocite and goethite were determined to the main phases[28]. This layer was not adhesive and was easily removed, and some of the corrosion products fell into the solution[29]. Thus, the corrosion products were likely not protective for the substrate. The SEM micrograph shown in Fig. 6a, needle-like and column-like corrosion products. EDS analysis of these two forms of corrosion products shows that iron and oxygen are the dominant components (Fig. 7), and it is inferred that the corrosion products were mainly iron oxides.

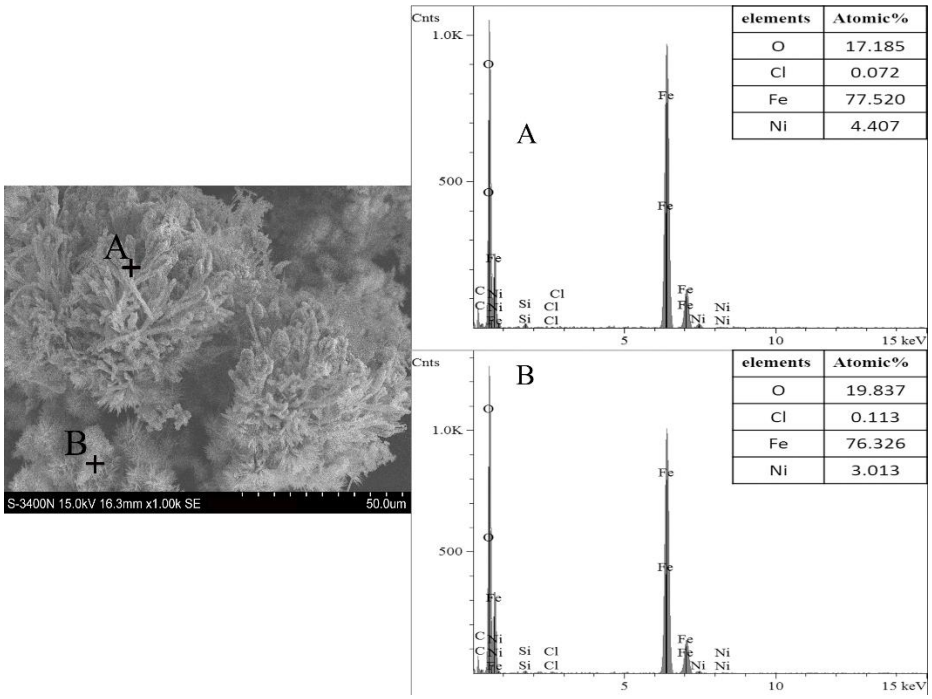

Figure 7. Microstructure and EDS spectra of corrosion products of 9 % Ni steel after immersion in 3.5 wt. % NaCl for 30 days

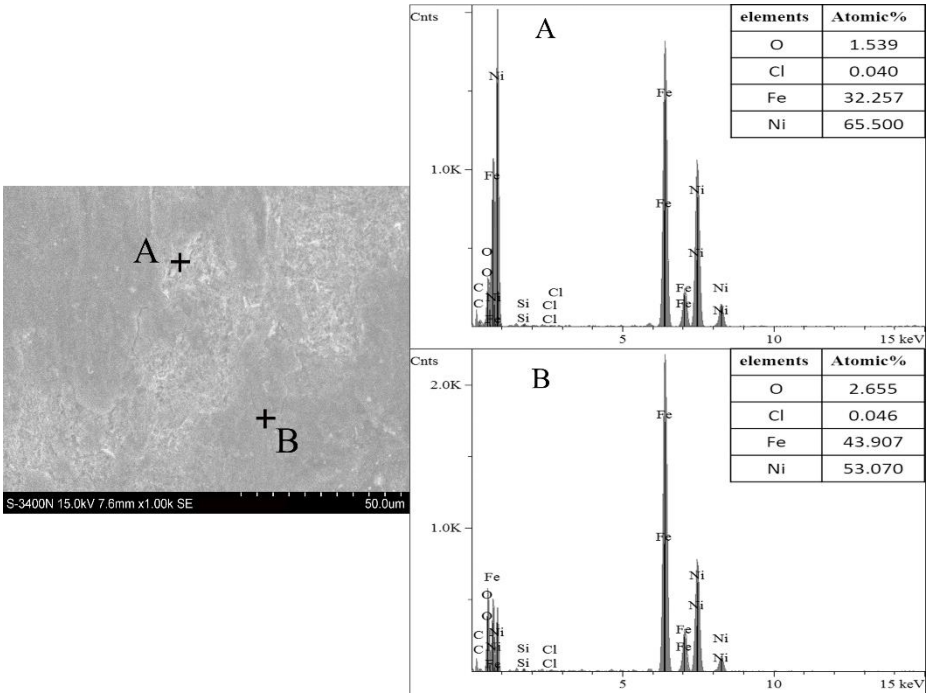

Figure 8. Microstructure and EDS spectra of the middle black layer of 9 % Ni steel after immersion in 3.5 wt. % NaCl for 30 days

XRD analysis of the powdered rust present on the steel indicated contents of lepidocrocite and goethite (shown in Fig. 10). These results indicate that the corrosion products were mainly γ-FeOOH (lepidocrocite), with trace α-FeOOH (goethite). Raman analysis also revealed the presence of γ-

FeOOH (lepidocrocite) and α-FeOOH (goethite) as shown in Fig. 11, which were identified by the bands at 250 cm^{-1}, 528 cm^{-1}, 655 cm^{-1} and 249 cm^{-1}, 307 cm^{-1}, 554 cm^{-1}, respectively[30]. The FTIR spectrum of corrosion products (Fig. 12) showed characteristic adsorption bands around 1020 cm^{-1} and 743 cm^{-1} corresponding to γ-FeOOH. The 3124 cm^{-1} adsorption band that was detected is related to the stretching vibration of the strong hydrogen bond formed between water molecules and hydroxyls, indicating that the corrosion products contained bound water. Because of the high sensitivity of magnetite to laser irradiation and poor crystallization, it was difficult to detect in the Raman and XRD spectra[31-33].

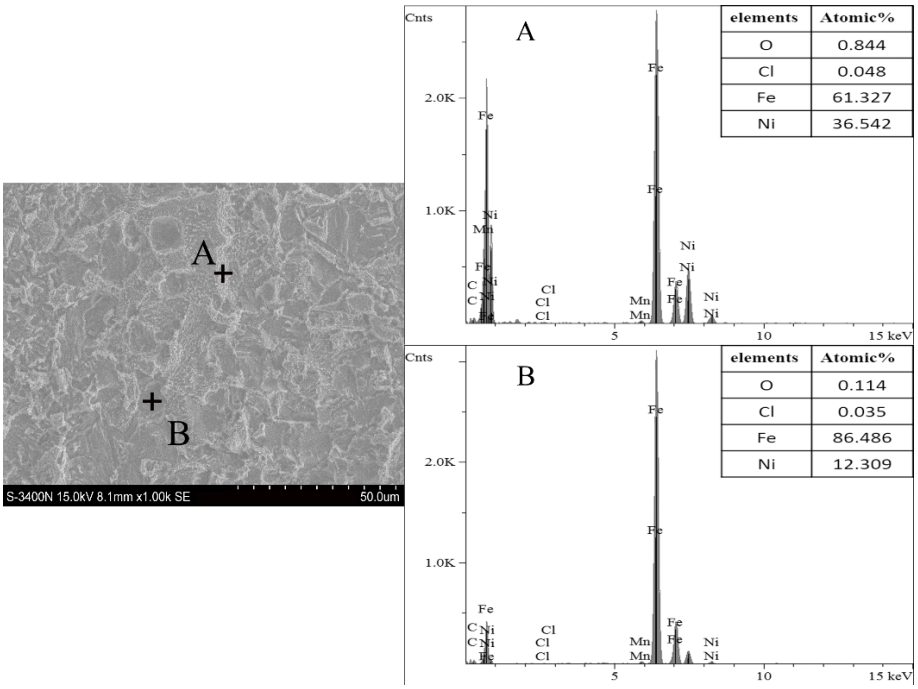

Figure 9. Microstructure and EDS spectra of the corroded surface (with corrosion products removed) of 9 % Ni steel after immersion in 3.5 wt. % NaCl for 30 days

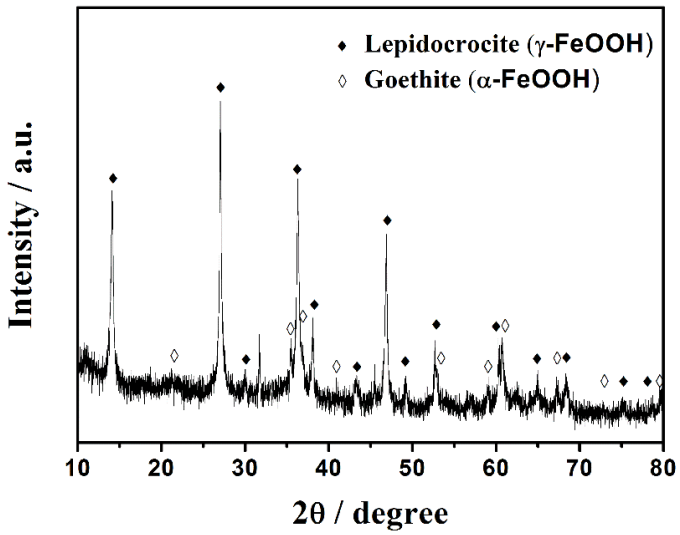

Figure 10. XRD spectrum of corrosion products of 9 % Ni steel after immersion in 3.5 wt. % NaCl for 30 days

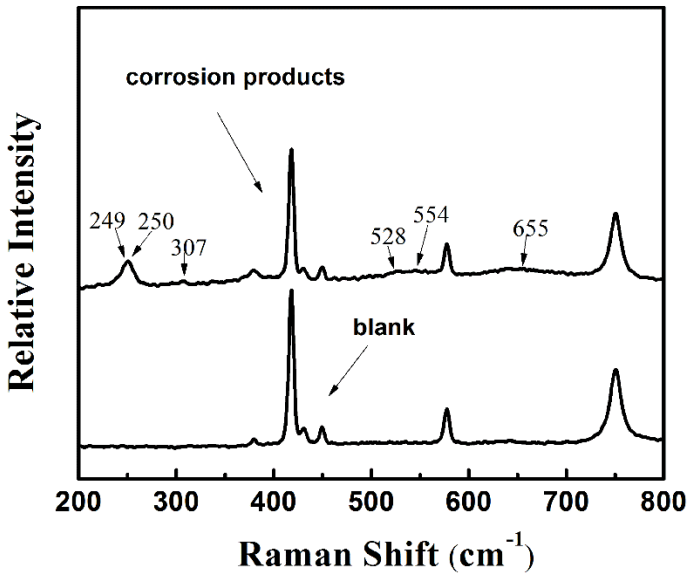

Figure 11. Raman spectrum of corrosion products of 9 % Ni steel after immersion in 3.5 wt. % NaCl over 30 days

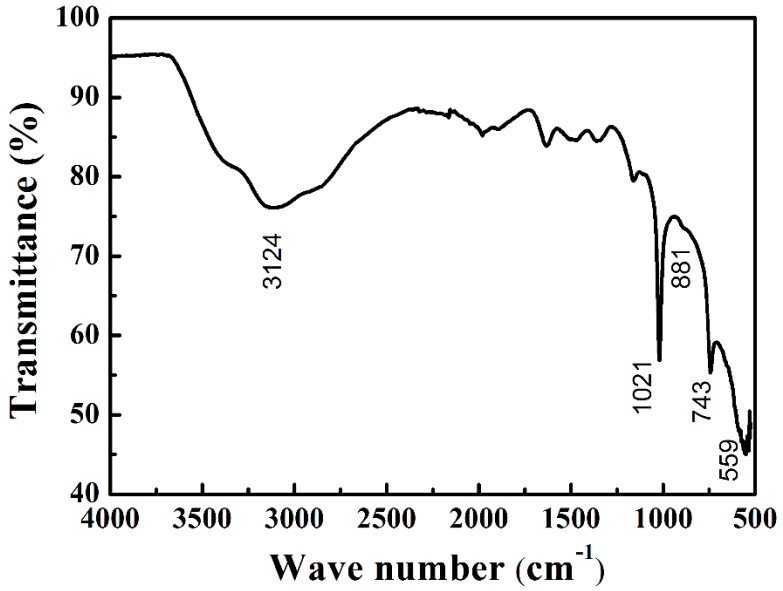

Figure 12. FTIR spectrum of corrosion products of 9 % Ni steel after immersion in 3.5 wt.% NaCl for 30 days

After removal of the outer corrosion products, there was an inner dense black layer below the brown yellow outer layer (shown in Fig. 6b); the black layer was thin and not adhesive. As shown in Fig. 8, EDS analysis revealed that this layer contained a large proportion of Ni, which must have originated from the metal matrix because of the absence of Ni in the 3.5 wt. % NaCl solution. Nickel is a stabilizing element in the metal matrix that is mainly intended to improve material toughness at low temperature, as well as to enhance corrosion resistance. However, in the electrolyte solution the presence of Ni accelerated the corrosion of the iron matrix because the electrochemical activity of Fe is

higher than Ni, causing the Fe to dissolve preferentially. Therefore, the Ni enrichment can be harmful to the material.

Fig. 6c shows the macroscopic corrosion morphology after the corrosion products were removed, which indicates that the corrosion is not uniform and has extensive but shallowly attacked areas. Fig. 9 shows EDS analysis of the substrate surface after removal of corrosion products, where iron and nickel account for a large proportion of the composition, but very little oxygen is detected. Moreover, the nickel content was higher in the bright areas than in the dark areas. According to the microstructure, the corrosion rate of the austenite phase enriched in nickel is lower than that of the martensite phase. Therefore, the dark areas were preferentially attacked; non-uniform corrosion occurred on the 9 % Ni steel surface.

4. CONCLUSIONS

The corrosion characteristics of 9 % Ni steel used for LNG storage tanks were studied in 3.5 wt. % NaCl solutions.

(1) Electrochemical tests revealed that the cathodic reaction of 9 % Ni steel in 3.5 wt. % NaCl was mainly the reduction of oxygen; a protective layer cannot be formed within 30 days.

(2) The microstructure of 9 % Ni steel consists of martensite and reverted austenite according to metallographic examination. The reverted austenite is rich in Ni, and the single-phase austenite and multi-phase martensite both account for the non-uniform corrosion of the metal.

(3) After 30 days of immersion, the loose outer corrosion products consisted mainly of lepidocrocite γ-FeOOH, trace goethite α-FeOOH and magnetite Fe_3O_4 as detected by EDS, XRD, FTIR and Raman analysis. Moreover, there was a nickel-rich layer below the loose corrosion layer. The presence of Ni sped up the corrosion of the Fe-matrix, because Fe is more chemically active than Ni, which may affect the service life of 9 % Ni steel.

ACKNOWLEDGMENTS

The authors wish to acknowledge the financial support of the work was support of the National Key Research and Development Program of China (Nos. 2017YFB0903700) and the National Science Foundation of China (Nos. 41276074).

References

1. S.H. Kim, C.Y. Kang, K.S. Bang, *J. Mater. Sci.*, 36 (2001) 1197.
2. O. Mattos, K.D. Assis, A. Zeemann, G. Zeemann, *Corrosion*, 73 (2017) 303.
3. C.K. Syn, J.W. Morris, S. Jin, *Metall. Trans. A*, 7 (1976) 1827.
4. A.R. Jarvis, J.H. Bulloch, *Int. J. Pres. Ves. Pip.*, 49 (1992) 271.
5. U. Ryuji, H. Yasushi, H. Takuya, I. Takehiro, S. Yasuhiro, I. Hiroshige, F. Hitoshi, *Nippon Steel Tech. Rep.*, 101 (2012) 68.
6. F. Lebel, E. Abi-Aad, B. Duponche, I.P. Serre, S. Ringot, P. Langry, A. Aboukaïs, *Mater. Des.*, 44 (2013) 283.

7. K.S.E. Al-Malahy, T. Hodgkiess, *Desalination*, 158 (2003) 35.
8. L. Bousselmi, C. Fiaud, B. Tribollet, E. Triki, *Corros. Sci.*, 39 (1997) 1711.
9. T. Kamimura, S. Hara, H. Miyuki, M. Yamashita, H. Uchida, *Corros. Sci.*, 48 (2006) 2799.
10. C. Re´mazeilles, Ph. Refait, *Corros. Sci.*, 49 (2007) 844.
11. Y. Ma, Y. Li, F. Wang, *Mater. Chem. Phys.*, 112 (2008) 844.
12. Sei J. Oh, D.C. Cook, H.E. Townsend, *Corros. Sci.*, 41 (1999) 1687.
13. K. Andreas, S. Udo, S. Joachim, *Steel Res. Int.*, 78 (2007) 189.
14. H.S. Shin, H.M. Lee, M.S. Kim, *Int. J. Impact Eng.*, 24 (2000) 571.
15. L.L. Machuca, L. Murray, R. G.ubner, S.I. Bailey, *Mater. Corros.*, 65 (2014) 8.
16. A.M Gatey, S.S. Hosmani, C.A. Figueroa. S.B. Arya, R.P. Singh, *Surf. Coat. Technol.*, 304 (2016) 413.
17. F.L. Xu, J.Z Duan, C.G Lin, B.R. Hou, *J. Iron Steel Res. Int.*, 22 (2015) 715.
18. N. Nakada, J. Syarif, T. Tsuchiyama, S. Takaki, *Mater. Sci. Eng., A*, 374 (2004) 137.
19. B. Fultz, J.I. Kim, Y.H. Kim, G.O. Fior, J.W. Morris, *Metall. Trans. A*, 16 (1985) 2237.
20. A.J. Abdalla, T.M. Hashimoto, C.M. Neto, M.S. Pereira, *Revista Brasileira Aplicacoes Vacuo*, 23 (2004) 52.
21. J.R. Li, Q.T. Jiang, H.Y. Sun, Y.T. Li, *Corros. Sci.*, 111 (2016) 288.
22. P. Liliana, S. Cristina, C.L. Virgil, M.L. Dan, S. Daniel, *Int. J. Electrochem. Sci.*, 13 (2018) 410.
23. J. Chen, Y. Zou, K. Matsuda, G. Zhao, *Int. J. Electrochem. Sci.*, 12 (2017) 1348.
24. H.Fr. Arendt, *Mater. Corros.*, 56 (2005) 271.
25. D. Kuang, Y.F. Cheng, *Corros. Sci.*, 99 (2015) 249.
26. C.X. Gu, Y.P. Zhu, S.M. Li, X.H. Ren, *Adv. Mater. Res.*, 1020 (2015) 1029.
27. L. Bousselmi, C. Fiaud, B. Tribollet, E. Triki, *Electrochim. Acta*, 44 (1999) 4357.
28. D. de la Fuente, J. Alcántara, B. Chico, I. Díaz, J.A. Jiménez, M. Morcillo, *Corros. Sci.*, 110 (2016) 253.
29. K.E. Garcı´a, A.L. Morales, C.A. Barrero, J.M. Greneche, *Corros. Sci.*, 48 (2006) 2813.
30. M.B. Leban, T. Kosec, *Eng. Fail. Anal.*, 79 (2017) 940.
31. S. Pineau, R. Sabot, L. Quillet, M. Jeannin, Ch. Caplat, I. Dupont-Morral, Ph. Refait, *Corros. Sci.*, 50 (2008) 1099.
32. Ph. Refait, M. Jeannin, R. Sabot, H. Antony, S. Pineau, *Corros. Sci.*, 71 (2013) 32.
33. Ph. Refait, M. Jeannin, R. Sabot, H. Antony, S. Pineau, *Corros. Sci.*, 90 (2015) 375.